

Accepted Manuscript

Investigation of the heat transfer properties of granular activated carbon with R723 for adsorption refrigeration and heat pump

M. Khaliji Oskouei, Z. Tamainot-Telto

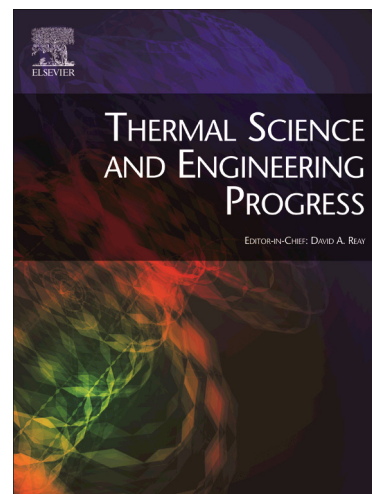
PII: S2451-9049(18)30530-4
DOI: <https://doi.org/10.1016/j.tsep.2019.05.003>
Reference: TSEP 353

To appear in: *Thermal Science and Engineering Progress*

Received Date: 4 September 2018
Revised Date: 9 May 2019
Accepted Date: 9 May 2019

Please cite this article as: M.K. Oskouei, Z. Tamainot-Telto, Investigation of the heat transfer properties of granular activated carbon with R723 for adsorption refrigeration and heat pump, *Thermal Science and Engineering Progress* (2019), doi: <https://doi.org/10.1016/j.tsep.2019.05.003>

This is a PDF file of an unedited manuscript that has been accepted for publication. As a service to our customers we are providing this early version of the manuscript. The manuscript will undergo copyediting, typesetting, and review of the resulting proof before it is published in its final form. Please note that during the production process errors may be discovered which could affect the content, and all legal disclaimers that apply to the journal pertain.



Investigation of the heat transfer properties of granular activated carbon with R723 for adsorption refrigeration and heat pump

M. Khaliji Oskouei and Z. Tamainot-Telto⁽¹⁾

School of Engineering, University of Warwick, Coventry CV4 7AL, UK

Abstract: This paper investigates the heat transfer coefficient of the wall to packed carbon contact (h) and the thermal conductivity of the packed bed (λ) by using parameters estimation method. A numerical heat conduction method was used in conjunction with an iterative process of minimizing the Mean Square Error (MSE) between both experimentally measured and model predicted temperatures in order to estimate h and λ parameters simultaneously. Experimental work was carried out by measuring the wall and centre temperatures of the sample reactor when suddenly submerged in a temperature controlled water bath at around 90°C. Four samples with packed bed density ranging from 600 kg m⁻³ to 750 kg m⁻³ were tested. The results for the GAC-R723 refrigerant pair show a quasi-linear increase in both thermal conductivity (λ) and wall contact heat transfer coefficient (h) with packed bed density. The thermal conductivity of GAC-R723 refrigerant varies between 0.77 W m⁻¹ K⁻¹ and 1.36 W m⁻¹ K⁻¹ (about three times the values without R723 refrigerant) while the wall contact heat transfer coefficient varied between 390 W m⁻² K⁻¹ and 735 W m⁻² K⁻¹ (up to 30% better than values without R723).

Keywords: Granular Activated Carbon; Adsorption, Ammonia (R717); Ammonia Blend (R723); Thermal Conductivity; Heat Transfer Coefficient.

Highlights:

- The thermal properties of packed granular activated carbon (GAC) and Ammonia Blend refrigerant (R723) are evaluated.
- A numerical method combined with experimental data was used.
- The thermal conductivity varies from 0.77 and 1.36 W m⁻¹ K⁻¹.
- The thermal conductivity is about three times the values without R723 refrigerant.
- The wall contact heat transfer coefficient varies between 390 and 735 W m⁻² K⁻¹ and is up to 30% better than values without R723 refrigerant.

⁽¹⁾ Corresponding author: E-mail z.tamainot-telto@warwick.ac.uk - Tel. +44 24 76522108 – Fax +44 24 76418922

NOMENCLATURE

A	Slope of the saturated liquid line for R723 on a Clapeyron diagram (K^{-1}); Heat transfer surface area (m^2)
C	Specific heat ($J\ kg^{-1}\ K^{-1}$)
CP	Overall specific heat ($J\ kg^{-1}\ K^{-1}$)
ΔP	Pressure change (Pa or bar)
Δr	Radius increment (m)
Δt	Time increment (s)
ΔT	Temperature change (K)
D	Diameter (m)
h	Heat transfer coefficient ($W\ m^{-2}\ K^{-1}$)
H	Heat of Sorption ($J\ K^{-1}$)
K	Dubinin-Astakhov coefficient
L	Length (m)
m	Mass (kg)
M	Mass (kg)
n	Dubinin-Astakhov coefficient
P	Pressure (Pa or bar)
r	Radius (m)
R	Gas constant ($J\ kg^{-1}\ K^{-1}$)
t	Time (s); Thickness (m)
T	Temperature (K or $^{\circ}C$)
U	Overall heat transfer coefficient ($W\ m^{-2}\ K^{-1}$)
UA	Overall heat transfer capacity ($W\ K^{-1}$)
x	Refrigerant concentration within the adsorbent ($kg\ kg^{-1}$)

Greek letters

λ Thermal conductivity ($\text{W m}^{-1} \text{K}^{-1}$)

ρ Density (kg m^{-3})

Subscripts

a Average

C Carbon

i Node reference number

j Reference number of data acquisitions

M Last node reference number

MSE Mean Square Error on temperature (K^2)

N Number of temperature data acquisitions per experimental test

o Maximum; Under saturation; Outer

p Under constant pressure

$R723$ Ammonia blend refrigerant

sat Under saturation conditions

Abbreviations

D-A Dubinin-Astakhov

DME Dimethyl Ether

GAC Granular Activated Carbon

ID Inner Diameter

OD Outer Diameter

R717 Ammonia refrigerant

R723 Ammonia blend refrigerant (60% R717 / 40% DME)

SEE Standard Estimated Error

V Valve

1. Background and Introduction

Granular activated carbon (GAC) is widely used in gas storage, industrial chemical process, food and beverage, environmental air and water treatments, personal protection equipment (PPE), metal recovery and medical treatments. However there are niche applications that are still under development namely refrigeration, heat pumping and energy storage that are more stringent in respect of its required thermo-physical characteristics. The thermal properties parameters play an important role in optimization of the adsorption generator cycling time; therefore wall contact heat transfer coefficient (h) and effective thermal conductivity (λ) are essential for cost effective design of thermal compressors. The heat transfer phenomenon is complex, in both the thermal generator and packed bed. Much of the literature concerns the heat transfer mechanisms through the heterogeneous granular activated carbon packed bed, with three major physical definitions such as: conduction through the grain, conduction through the grain to grain contact area, conduction and convection through the gas and condensed liquid and radiation heat transfer through the grain surface and void. **Figure 1** illustrates some of the heat transfer mechanisms suggested by Argo and Smith [1], Yagi and Kunni [2], and also by Calderbank and Progoriski [3] for packed beds.

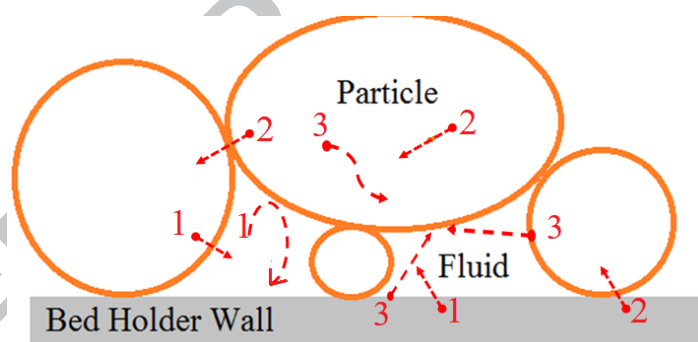


Figure 1: Heat transfer phenomena in the packed bed.

Table 1 provides a summary of heat transfer mechanisms, which reflect the complexity of heat transfer in a packed bed as illustrated by **Figure 1**

Radiation is the dominant heat transfer mechanism through the granular bed under high vacuum and at high temperatures [4]. The convection effect between particle and wall is increased by the desorption process, while it is possible to neglect the convective heat flow according to pore size [4]. The temperature gradient in the thermal generator, due to the desorption process, will cause the system pressure to increase. Therefore, by increasing system pressure, the overall heat transfer effect will increase.

Table 1: Heat transfer mechanisms in the thermal generator and packed bed.

Heat Transfer Mechanism	Governing Modes
1- Convection	a. Particle – fluid
	b. Wall – fluid
	c. Fluid – fluid (fluid mixing)
2- Conduction	a. Through the particle
	b. Particle – particle
	c. Gas layer around the particle – particle
	d. Stagnant gas (gas – particle)
	e. Wall – particle
3- Radiation	a. Grain surface – grain surface
	b. Grain surface - Wall
	c. Neighbouring voids (void – void)

The two conduction heat transfer mechanisms, particle-to-particle and particle surrounded gas layer-to-particle, act in parallel in the granular packed bed. The particle-to-particle and particle surrounded gas layer-to-particle mechanisms act in series with conduction through the particles. Therefore, both mechanisms can be observed in conduction through the particle mechanism [5]. The other two remaining conduction mechanisms, gas-to-particle and wall-to-particle, have only a small effect on the heat transfer through the granular packed bed. Therefore it is possible to remove them from heat transfer modelling [6].

The objective of this study is to investigate the heat transfer properties of packed Granular Activated Carbon (GAC) with Ammonia blend refrigerant (R723) for adsorption refrigeration, heat pumping and energy storage applications.

2. Research Methodology

The complexity of heat transfer in porous media shows the necessity of finding an experimental and analytical procedure able to reflect packed bed heat transfer characteristics in a thermal generator, without including separately each individual mode outlined in **Table 1**. Instead, we have considered a lumped heat transfer model characterised by both wall contact (combined adsorbent-refrigerant) heat transfer coefficient (h) and bed effective thermal conductivity (λ). In order to estimate those two key heat transfer characteristics, a combination of experimental and numerical methods could simulate the actual behaviour of a GAC packed bed in the presence of R723. Therefore, Smoluchowski's adopted measurement

methodology along with a one-dimensional transient numerical method was used. Regarding Smoluchowski's measurement methodology, the granular material was placed within a cylindrical sample holder [7]. The sample holder length must be approximately ten times higher than the outside diameter in order to satisfy the one-dimensional heat transfer conditions. To measure the temperature jump and disturbance at the surface and centre of the cylindrical sample holder, two thermocouples were placed at both the external surface and centre of the sample holder as illustrated in **Figure 2**.

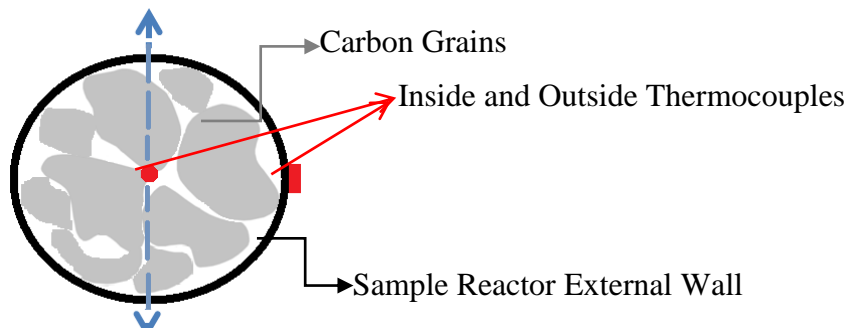


Figure 2: Cross section of tubular sample holder with thermocouples [7]

The estimation of the thermo-physical properties of the granular packed bed, namely the wall contact heat transfer coefficient (h) and effective thermal conductivity (λ) is based on two stages:

Stage 1: The first stage was the direct explicit numerical method based on both energy and mass balance laws aimed to determine the transient temperature profile of the material by imposing the sudden change in temperature on the reactor's (sample holder) wall.

Stage 2: The second step consists of a computational algorithm which identifies the thermo-physical properties (h and λ) of GAC in the course of comparing the predicted and the measured transient temperature profile in the centre $T(r_M, t)$ through the minimization of the Mean Square Error (MSE):

$$\text{MSE} = \frac{1}{N} \sum_{j=1}^N (T_{\text{calculated } j} - T_{\text{experimental } j})^2 \quad (1)$$

2.1 Explicit numerical equations

Figure 3 shows the domain discretization and location of the imaginary nodes in the half of cylindrical sample holder. Heat is flowing into the packed bed from the top (outside the sample holder wall) into the bottom (centre of sample holder), which is represented by the

symmetry line in the sample. Node 1 is allocated to the heating area, and node 2 is assumed to be attached to the outside wall of the cylindrical holder. The outside thermocouple displays the temperature at node 2. To simplify the modelling process, we assume that the temperatures at nodes 1 and 2 are identical.

Equation 2 shows the one-dimensional domain discretization for the energy balance over the specific volume, which is illustrated in **Figure 3**, at the carbon packed bed. The temperature changes over a specific volume at a specified time step, which is connected to the temperature and thermal resistance of the nodes towards the inner (west) and outer (east) of the cylinder, for the same time step.

$$UA\Delta T = M_{Carbon} [C_{P,Carbon} + xC_{P,R723\ Liquid}] \frac{\Delta T}{\Delta t} - H \frac{\Delta m_{R723}}{\Delta t} \quad (2)$$

UA is the overall heat transfer capacity. The overall heat transfer capacity for each energy balance line is divided across the two sections. The thermal resistance which the heat flow faces when traveling from the left (west) to the right (east) boundary and vice versa is called west (UAwest) and east (UAeast) overall heat transfer capacities, respectively (see Figure .3 b). The values of UAwest and UAeast in **Equation 3** are divided into three regions. The first region is a node on the carbon surface in the vicinity of the sample holder wall from the inside; the second region involves the inner nodes and the final is the centre node. Also, M_{Carbon} is the mass of the carbon for each representing cell. Therefore, it could also be written as the following discretized energy balance equation:

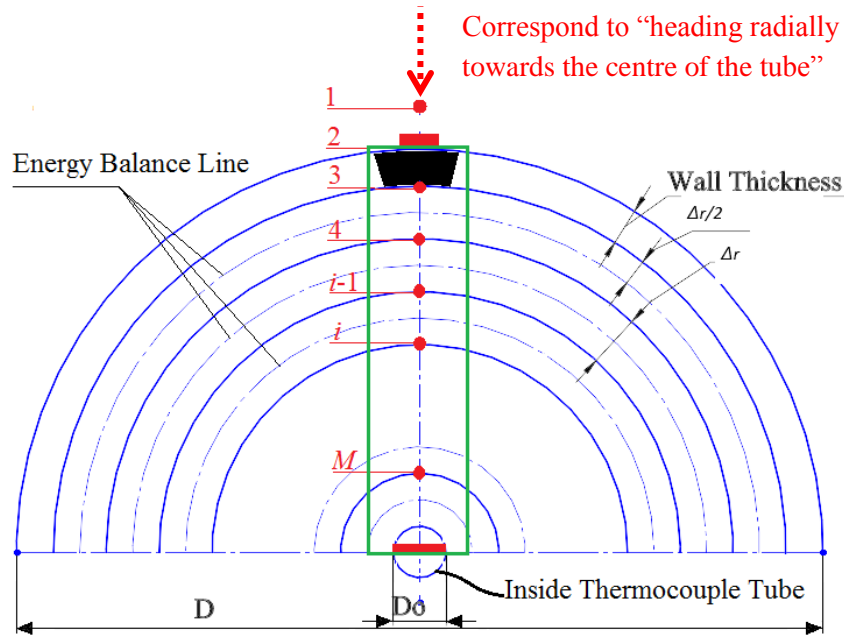
$$UA * \Delta T = UA_{west} * [T_{i-1}^t - T_i^t] + UA_{east} * [T_{i+1}^t - T_i^t] \quad (3)$$

Appendix A shows the energy balance, overall heat transfer coefficient and represented cell's carbon masses in all three regions.

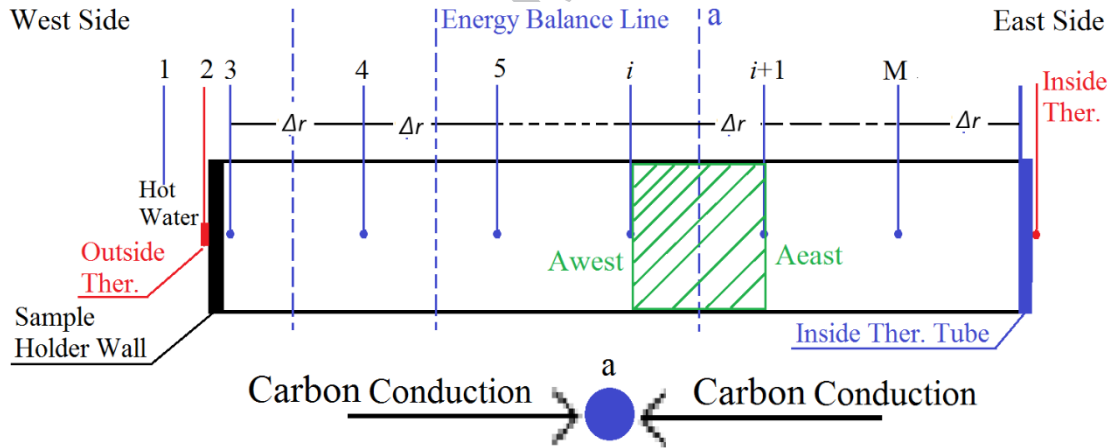
The effective specific heat of the sample with adsorbed R723 was calculated from the following expression:

$$CP = C_{P-Carbon} + xC_{P-R723\ Liquid} \quad (4)$$

Where $C_{p-Carbon}$ and $C_{p-R723Liquid}$ are the specific heat of the GAC and liquid R723, respectively. To simplify the modelling both specific heats are assumed to be constant: $C_{p-Carbon} = 1125 \text{ J kg}^{-1} \text{ K}^{-1}$ and $C_{p-R723Liquid} = 4500 \text{ J kg}^{-1} \text{ K}^{-1}$ in the temperature range of the thermal conductivity test.



(a) Top view



(b) Side view

Figure 3: Illustration (half cross-section) of the domain discretization for energy balance in the packed carbon in a one-dimensional cylindrical configuration.

The value $x_{C_{p-R723Liquid}}$ is the R723 adsorbed phase contribution with the concentration x , calculated from Dubinin-Astakhov (D-A) [8]:

$$x = x_0 \exp \left[-K \left(\frac{T}{T_{sat}} - 1 \right)^n \right] \quad (5)$$

where T is the sample temperature (K), T_{sat} (K) is the saturation temperature corresponding to the gas pressure P , x_o is the concentration of R723 under saturation conditions corresponding to the maximum concentration (0.354 kg kg^{-1}), K is 3.7342 and n is 1.187 [9].

The value ΔT is temperature change over the represented cell of carbon between the two nodes.

$H \frac{\Delta m_{R723}}{\Delta t}$ is a heat rate generation term in the represented cell in **Equation 2**. H is the heat of the sorption and is given by the following expression [10]:

$$H = RA \frac{T}{T_{sat}} \quad (6)$$

where R is the gas constant ($364.2 \text{ J kg}^{-1} \text{ K}^{-1}$), T is the sample temperature (K), T_{sat} (K) is the saturation temperature corresponding to the gas pressure P and A corresponds to the slope of saturated liquid line on a plot of $\ln(P)$ vs. $-1/T_{sat}$ or Clapeyron diagram ($A = 2621.3 \text{ K}^{-1}$).

The term $\Delta m_{R723}/\Delta t$ in **Equation 2** corresponds to the change of the adsorbed refrigerant mass in the carbon for the represented cells over time. The mass of the adsorbed refrigerant gas, the gas which is condensed in the activated carbon pores, per mass of carbon, is called concentration x (kg of adsorbate per kg of adsorbent or kg kg^{-1}):

$$x = \frac{m_{R723}}{M_{Carbon}} \rightarrow m_{R723} = xM_{Carbon} \rightarrow \frac{\Delta m_{R723}}{\Delta t} = \frac{\Delta x}{\Delta t} M_{Carbon} \quad (7)$$

Equation 7 shows the relationship between the mass of adsorbed refrigerant and the mass of adsorbent (GAC) and concentration. Then it is possible to rewrite **Equation 6**:

$$\frac{\Delta m_{R723}}{\Delta t} = M_{Carbon} \frac{\Delta x}{\Delta t} \quad (8)$$

Regarding the D-A **Equation 5**, the concentration depends on sample temperature and pressure. Therefore, in **Equation 8** the differentiation of concentration change by time based on partial differential rules, is rewritten as while assuming a quasi-equilibrium of the discretized sample control volume:

$$\frac{\Delta x}{\Delta t} = \frac{\Delta x}{\Delta T} \frac{dT}{dt} + \frac{\Delta x}{\Delta P} \frac{dP}{dt} \quad (9)$$

In the D-A equation, the pressure is represented by T_{sat} ($\Delta P \propto \Delta T_{sat}$). Therefore **Equation 9** becomes:

$$\frac{\Delta x}{\Delta t} = \frac{\Delta x}{\Delta T} \frac{\Delta T}{\Delta t} + \frac{\Delta x}{\Delta T_{sat}} \frac{\Delta T_{sat}}{\Delta t} \quad (10)$$

Equation 10 shows the differentiation of **Equation 5** (D-A Equation) with respect to the sample temperature and saturation temperature:

$$\frac{\Delta x}{\Delta T} = -\frac{Kn x}{T_{sat}} \left(\frac{T}{T_{sat}} - 1 \right)^{n-1} \quad \frac{\Delta x}{\Delta T_{sat}} = Kn x \frac{T}{T_{sat}^2} \left(\frac{T}{T_{sat}} - 1 \right)^{n-1} \quad (11)$$

Finally, substituting **Equation 11** into **Equation 10**, it could be written as follows:

$$\frac{\Delta x}{\Delta t} = \left[-\frac{Kn x}{T_{sat}} \left(\frac{T}{T_{sat}} - 1 \right)^{n-1} \right] \frac{\Delta T}{\Delta t} + \left[Kn x \frac{T}{T_{sat}^2} \left(\frac{T}{T_{sat}} - 1 \right)^{n-1} \right] \frac{\Delta T_{sat}}{\Delta t} \quad (12)$$

This would be the result of substituting all those equations which have been mentioned above with **Equation 2**, and rearranging it for the discretized domain and time:

$$\frac{\frac{UA\Delta T}{M_{Carbon}} \Delta t + \left(RA \frac{T_i^t}{T_{sat}^t} \right) \left[Kn x_i^t \frac{T_i^t}{T_{sat}^t} \left(\frac{T_i^t}{T_{sat}^t} - 1 \right)^{n-1} \right] (T_{sat}^{t+1} - T_{sat}^t)}{(CP) - \left(RA \frac{T_i^t}{T_{sat}^t} \right) \left[-\frac{Kn x_i^t}{T_{sat}^t} \left(\frac{T_i^t}{T_{sat}^t} - 1 \right)^{n-1} \right]} + T_i^t = T_i^{t+1} \quad (13)$$

Appendix B shows the detailed equations leading to **Equation 13** by substituting all mentioned equations into **Equation 2**.

2.2 Sample preparation

Based on the main concept, the sample holder was made from stainless steel with an outside diameter of 1", 0.71 mm wall thickness and 200 mm length, to satisfy the one-dimensional conditions. 208-C granular activated carbon from Chemviron Carbon Ltd with 13×30 US sieve mesh size (1.5 mm × 0.6 mm) is held in place by welding two caps on the top and bottom of the cylinder (**Figure 4**). A small stainless-steel tube, which is called thermocouple tube, with 1/8" OD and 0.56 mm wall thickness, was welded to the top cap. The thermocouple tube was located in the middle of the sample holder with 100 mm distance from the top cap surface. This tube was used to pass the thermocouple into the centre of the sample holder in order measure the packed bed centre temperature. The second thermocouple was attached to the cylinder wall from the outside at the same height as the internal thermocouple. The outside thermocouple measures the temperature at the boundary wall. Four identical sample holders with packed activated carbon with density of 625.9 kg m⁻³, 661.8 kg m⁻³, 707.7 kg m⁻³ and 749.7 kg m⁻³ were prepared. **Figure 5** shows the sample module, with the location of the two K-type thermocouples. One thermocouple was attached

to the sample surface while another was passed into the centre of the sample through the thermocouple tube. Each sample module was isolated after vacuuming and charging with refrigerant using a Swagelok $\frac{1}{4}$ " 316 stainless steel "M" series metering (needle) valve.

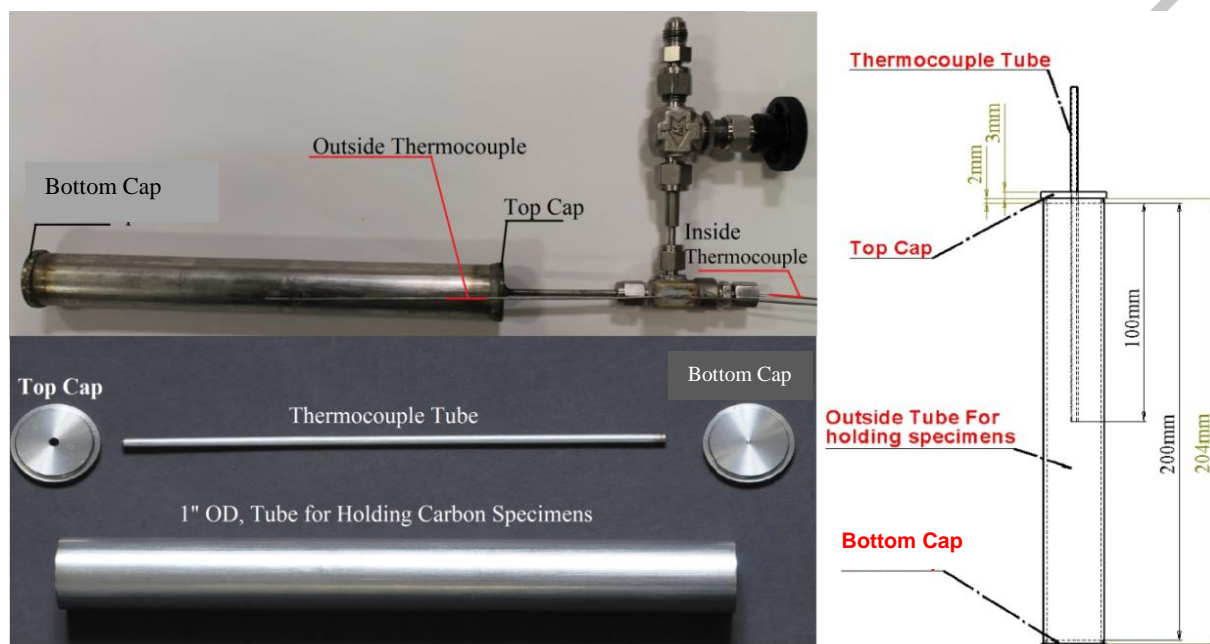


Figure 4: Packed GAC sample holder

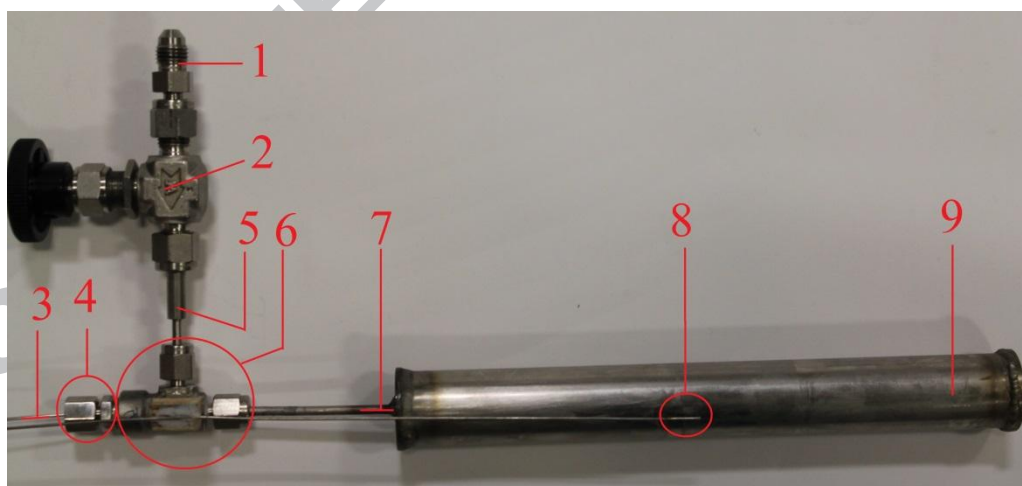


Figure 5: Sample holder general view with part details. 1: $\frac{1}{4}$ " filler to connect in to the vacuum and charging manifold hose, 2: Swagelok $\frac{1}{4}$ " 316 stainless steel "M" series metering (needle) valve for module isolation, 3: Inside thermocouple, 4: 316 stainless steel $\frac{1}{8}$ " compression fitting to seal the thermocouple, 5: $\frac{1}{8}$ " connection to $\frac{1}{4}$ ", 6: Swagelok 316 stainless $\frac{1}{8}$ " female run tee, 7: Thermocouple tube with $\frac{1}{8}$ " OD, 8: Outside thermocouple and attaching position, 9: Sample holder.

2.3 Experimental set-up and test procedure

The schematic of the experimental set-up is shown in **Figure 6**: it mainly consists of the sample holder linked to a receiver via connecting tubes and valves. The experimental procedure consists of suddenly plunging the sample that was initially at ambient temperature into the hot water bath. Prior to this test, the needle valve (V1) was fully open. The hot water bath has thermostatic control. The bath temperature was set to 90°C. Three thermocouples were located at different heights in the thermal bath to monitor the water temperature uniformity at different levels. The Strawberry Tree data shuttle, in association with Workbench software, was used to record the experimental data with an interval time of 0.15 second.

To remove moisture and air from the system, the sample holder was heated to 200°C while being kept under the vacuum for 24 hours in an oven. The sample module weight was measured before and after the drying process, to find out the actual amount of dried carbon in the sample.

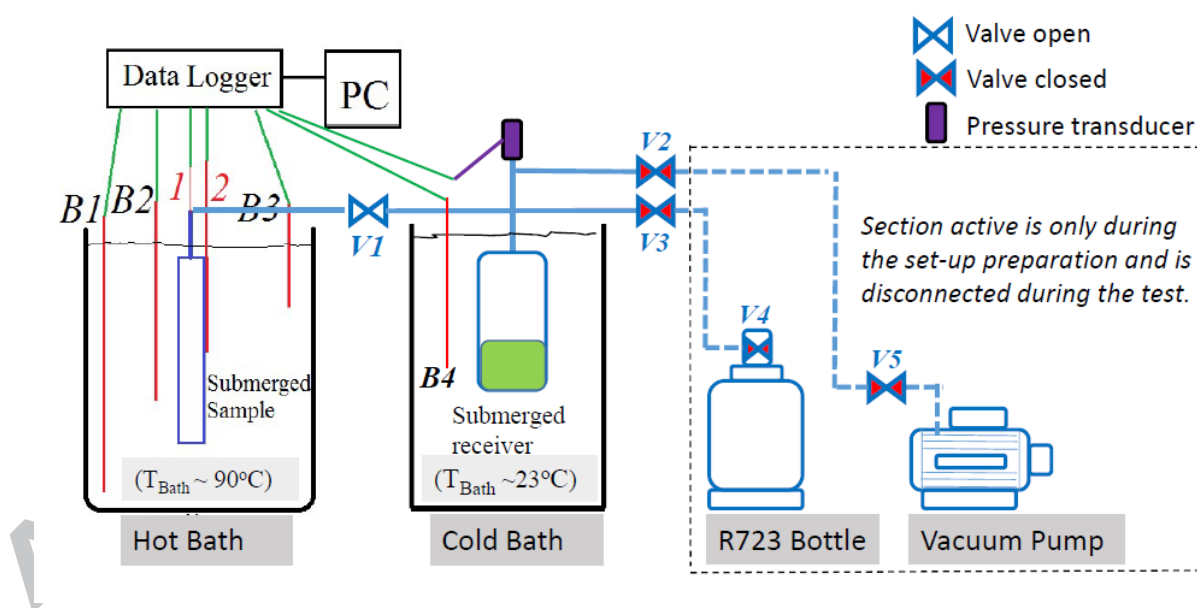


Figure 6: Schematic diagram of experimental set-up (allocated thermocouples: in baths (B1, B2, B3 and B4), sample centre thermocouple (1), sample outside thermocouple (2)).

To charge the sample module with refrigerant, a receiver was used. The receiver was initially charged with about 61.3 g and 20% extra from the refrigerant's main cylinder. The vessel is connected to the sample module using about 250 mm long stainless steel tube with ¼" OD and 0.71 mm thickness. The connection line and sample module were initially evacuated

using a vacuum pump for 30 minutes at room temperature. The main Swagelok ¼” 316 stainless steel “M” series metering (needle) valve V2 for module isolation was opened and closed slowly during the vacuum process (while V1 and V5 are open and V3 and V4 closed). The status of all valves during different operating conditions are summed up in **Table 2**.

Table 2: Valves status vs. operating conditions

Valve Operation	V1	V2	V3	V4	V5
Vacuum	Open	Open	Open	Closed	Open
R723 loading	Open	Closed	Open	Open	Closed
Test	Open	Closed	Closed	Closed	Closed

After about 12 hours, the sample reactor was stabilised in terms of both pressure and temperature, after which both sample module and receiver were suddenly and simultaneously submerged into the hot water bath and cold water bath respectively. The pressure and temperatures were recorded and stored in a data file every 0.15 second until the centre temperature reached the hot bath set temperature within $\pm 0.5^{\circ}\text{C}$.

The photograph of the top view of the experimental set-up is shown in **Figure 7** highlighting all relevant components including thermocouples and the pressure transducer.

By setting up the time step ($\Delta t = 1$ second) and length step ($\Delta r = 0.882$ mm corresponding to 10 layers of activated carbon) for simulation tests, the temperature of each node was calculated using the given values of wall contact heat transfer coefficient (h) and intrinsic thermal conductivity (λ). Finally, to identify appropriate values of h and λ for each density, the modelled temperature profile of the centre node was compared with the experimental data for the same node by minimizing the Mean Square Error (MSE) as defined in **Equation 1**. The full program for both simulation and estimation of heat transfer characteristics (h and λ) was written in MATLAB R2012b.

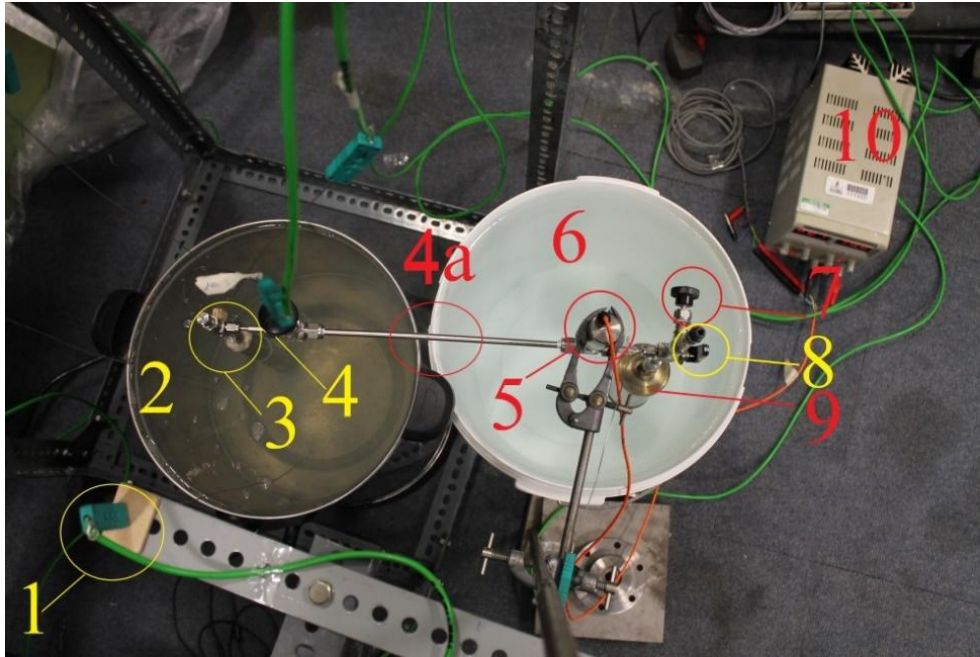


Figure 7: Top view of experimental set-up. 1: Thermal bath K type thermocouple, 2: Hot water thermal bath with build in thermostat, 3: Sample module with inside & outside thermocouples, 4: Swagelok ¼” 316 stainless steel “M” series metering (needle) valve for module isolation, 4a: ¼” connection tube, 5: Druck four wire pressure transducer, 6: Water bath to keep condensing vessel at steady temperature situation, 7: Swagelok 1/8” 316 stainless steel “M” series metering (needle) valve for vacuum line isolation, 8: 1/8” on & off Swagelok three ways valve and 1/8” filler to connect to the vacuum and vacuum line, 9: Condenser & charging vessel, 10: Precision adjustable power supply.

3. Results and discussion

Figure 8 and **Figure 9** show the temperature and pressure profiles with minimum (625.9 kg m^{-3}) and maximum (749.8 kg m^{-3}) densities, respectively. The difference between the experimental data and model predictions of the temperature in the centre was well minimised.

Figure 10 presents an illustrative example the variation of *MSE* values function of the number of simulation runs that were explored for the first sample (density 625.9 kg m^{-3}) in a range of $0.01 \text{ W m}^{-1} \text{ K}^{-1} < \lambda < 1.5 \text{ W m}^{-1} \text{ K}^{-1}$ with an increment of $0.01 \text{ W m}^{-1} \text{ K}^{-1}$ and $50 \text{ W m}^{-2} \text{ K}^{-1} < h < 1000 \text{ W m}^{-2} \text{ K}^{-1}$ with an increment of $1 \text{ W m}^{-2} \text{ K}^{-1}$. For this particular density, the minimum *MSE* was obtained from the minimization process as 0.3557 corresponding to $\lambda = 0.77 \text{ W m}^{-1} \text{ K}^{-1}$ and $h = 390 \text{ W m}^{-2} \text{ K}^{-1}$. During the test with all module samples, from an initial temperature of about 25°C and pressure of about 9.9 bar, the experiments reach the same centre temperature (about 90°C) and system pressure (about 10.7 bar via a maximum

value of about 11.9 bar). As expected by increasing the packed bed density from 625.9 kg m^{-3} to 749.7 kg m^{-3} , the time to reach the steady state decreases from about 850 seconds to 650 seconds.

All samples were tested and the final results of the thermal conductivity (λ) and wall contact heat transfer coefficient (h) were identified: all results are summed up in **Table 3**. Overall, a fairly good fit with a minimum *MSE* was obtained for each packed density of activated carbon.

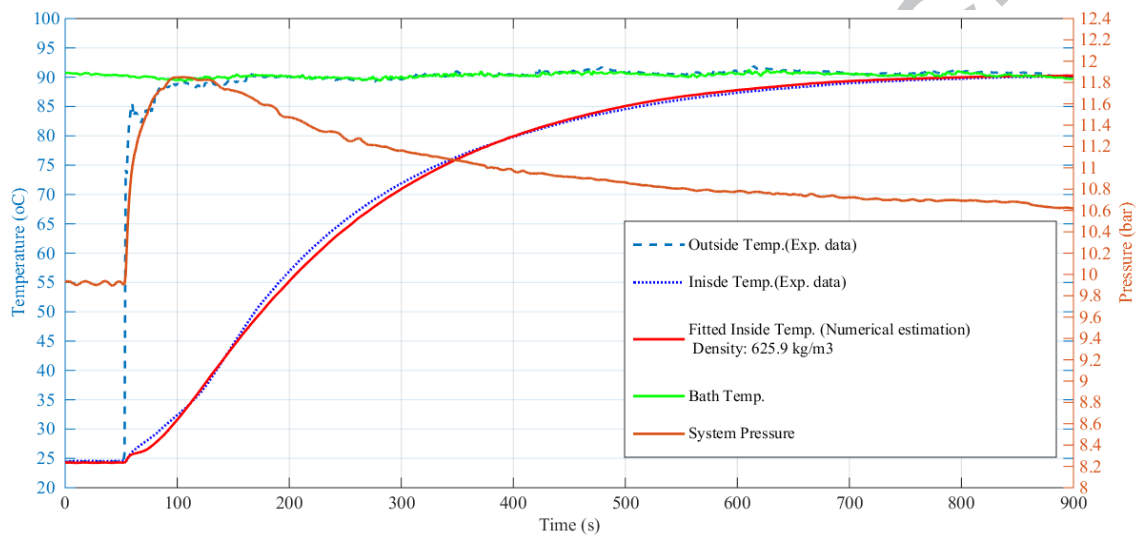


Figure 8: Temperature and pressure profiles for activated carbon-R723 pair with packed density of 625.9 kg.m^{-3} ($\lambda = 0.77 \text{ W m}^{-1} \text{ K}^{-1}$ and $h = 390 \text{ W m}^{-2} \text{ K}^{-1}$)

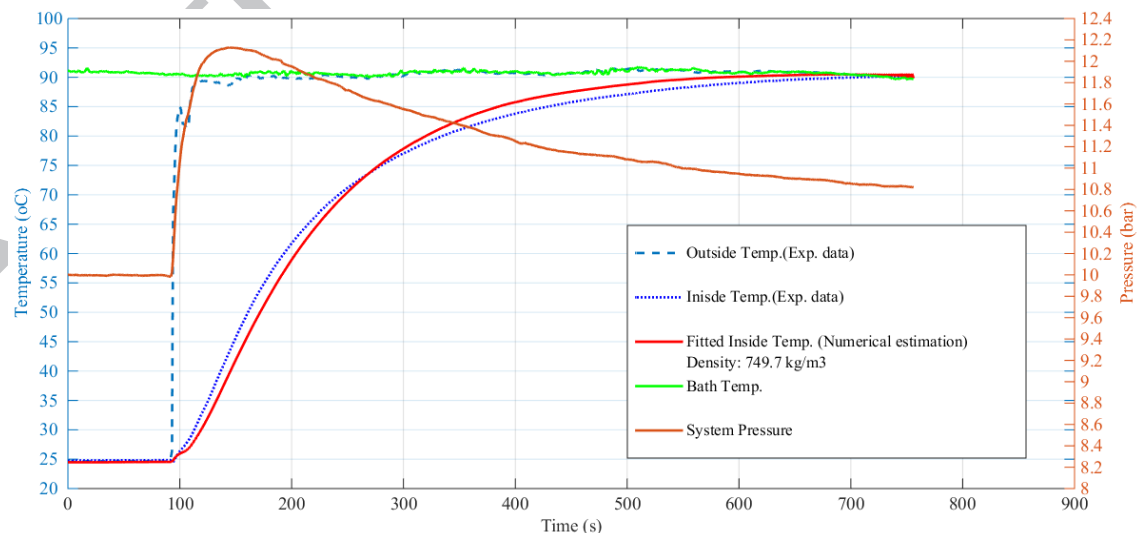


Figure 9: Temperature and pressure profiles for activated carbon-R723 pair with packed density of 749.7 kg.m^{-3} ($\lambda = 1.36 \text{ W m}^{-1} \text{ K}^{-1}$ and $h = 735 \text{ W m}^{-2} \text{ K}^{-1}$)

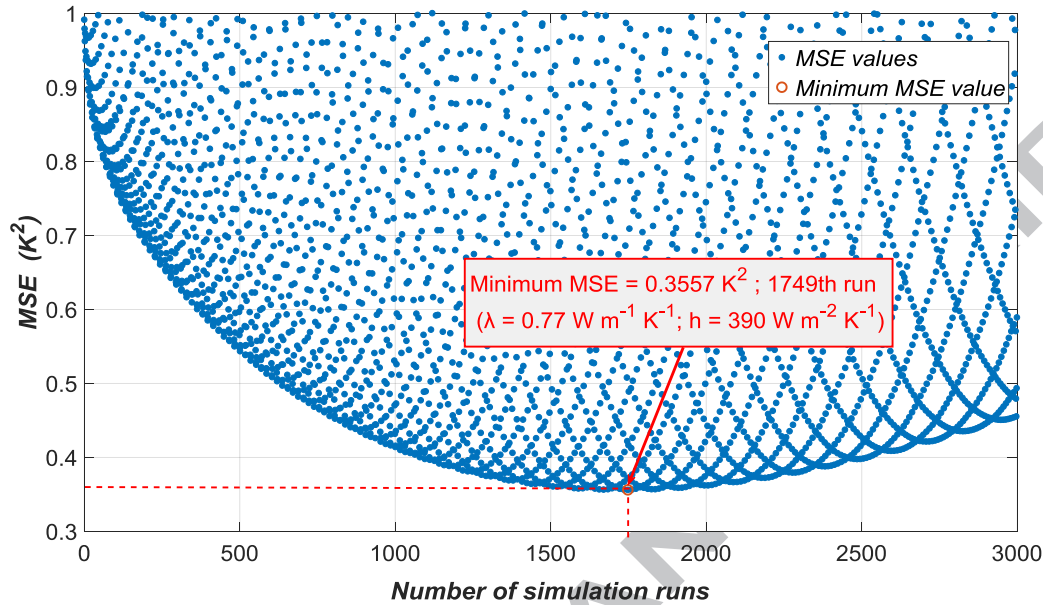


Figure 10: MSE values for activated carbon-R723 pair with packed density of 625.9 kg m^{-3} function of the number simulation runs - Each simulation run corresponds to a given (λ, h) pair.

Table 3: Summary of thermal properties of Granular activated carbon packed - R723 pairs.

<i>Carbon Density</i>	λ	h	<i>MSE (K²)</i>
<i>kg m⁻³</i>	<i>W m⁻¹ K⁻¹</i>	<i>W m⁻² K⁻¹</i>	
625.9	0.77	390	0.3557
661.8	1.19	451	0.8498
707.7	1.26	536	0.7063
749.8	1.36	735	0.6982

Figure 11 shows the average concentration of R723 in granular activated carbon. For all densities, the average concentration is fairly constant, as expected, because the operating conditions (pressure and temperature) are nearly the same for all modules: the difference of average concentration between the minimum (625.9 kg m^{-3}) and maximum (749.7 kg m^{-3}) densities is around 2%.

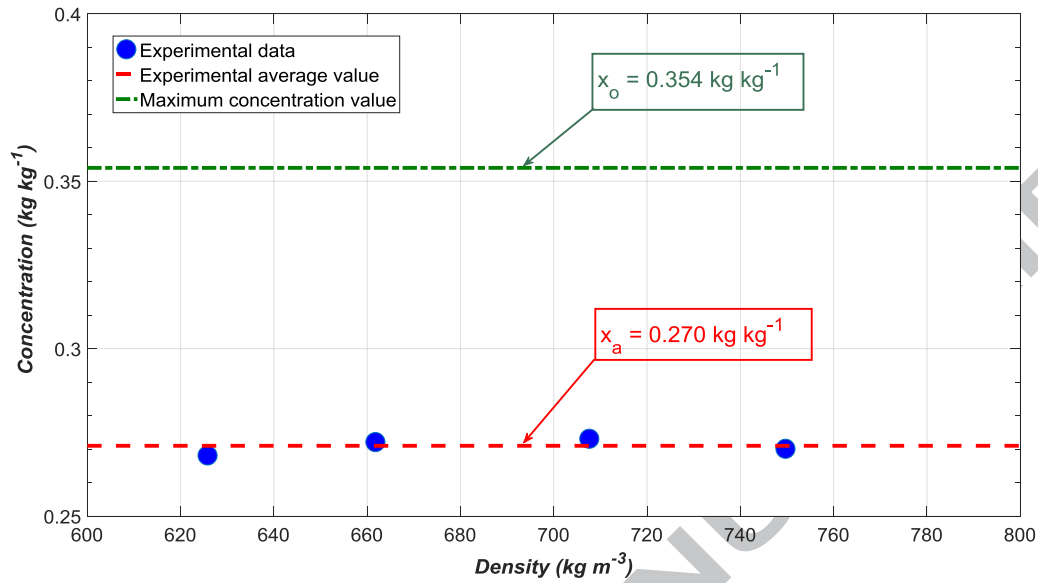


Figure 11: The average concentration of R723 in granular activated carbon packed bed

(Bed temperature variation: 25°C to 90°C; Bed pressure variation: 8 bar to 12 bar).

Figure 12 and **Figure 13** show the thermal conductivity (λ) and wall contact heat transfer coefficient (h), respectively, as a function of the packed carbon density. As expected, both thermal conductivity (λ) and heat transfer coefficient (h) increase quasi-linearly with density. Those results are also compared with preliminary tests carried out (using the same samples and methodology) without the refrigerant R723 corresponding to tests in atmospheric pressure. However both maximum concentration x_o and heat of the sorption H were assumed to be zero in all relevant equations leading to the identification of both thermal conductivity (λ) and wall contact heat transfer (h) [11].

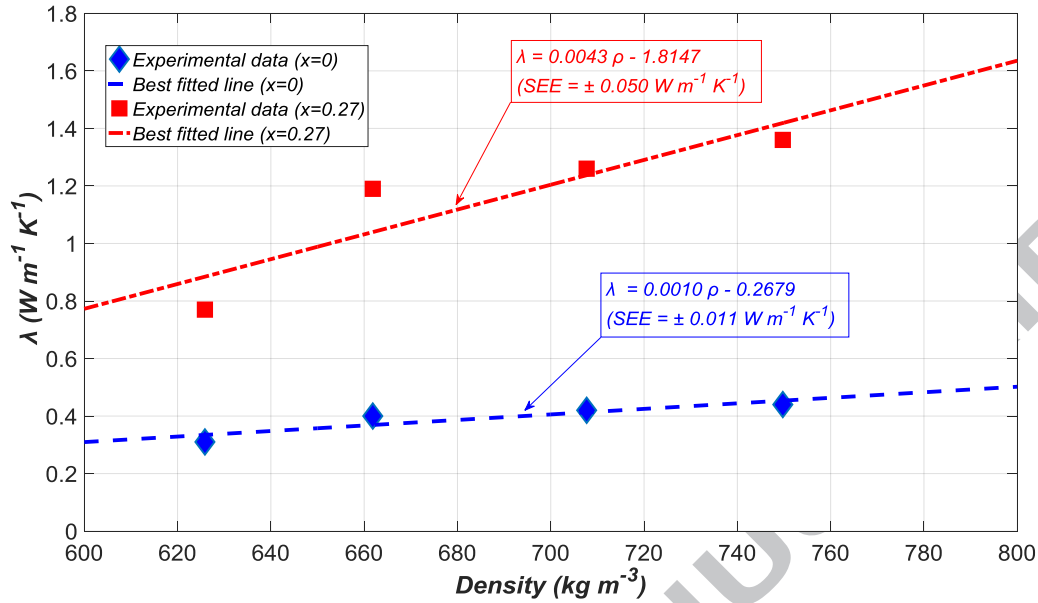


Figure 12: Experimental thermal conductivity of packed bed with and out refrigerant R723

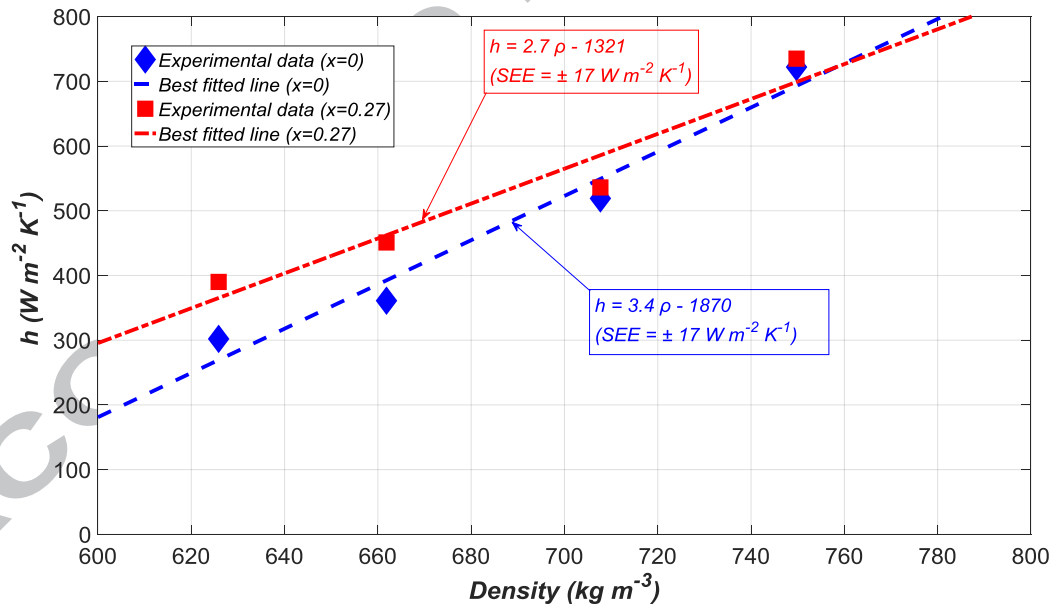


Figure 13: Experimental wall contact heat transfer coefficient with and without refrigerant R723.

For packed bed densities of 625.9 kg m^{-3} and 749.7 kg m^{-3} , the effective thermal conductivity ' λ ' of GAC without refrigerant increases from $0.31 \text{ W m}^{-1} \text{K}^{-1}$ to $0.44 \text{ W m}^{-1} \text{K}^{-1}$, which is well within the range expected [12], while for the packed GAC with refrigerant R723 (with

an average concentration of 27% in mass) it increases from $0.77 \text{ W m}^{-1} \text{ K}^{-1}$ to $1.36 \text{ W m}^{-1} \text{ K}^{-1}$. The presence of refrigerant increases the effective thermal conductivity by a factor of about 3. In fact, due to the small pressure swing of the refrigerant during the tests (maximum 2 bar), the packed GAC bed will remain with high concentration of refrigerant. Since the adsorbed refrigerant is assumed to be in a liquid form that is well bonded on the wall of micro-pores by the means of Van der Waals forces, this enhances the effective thermal conductivity of the packed bed more than the gas in the inter-grains space. However for the same density range, the wall contact heat transfer coefficients ' h ' for GAC with refrigerant varies from $302 \text{ W m}^{-2} \text{ K}^{-1}$ to $722 \text{ W m}^{-2} \text{ K}^{-1}$, while for the GAC with refrigerant R723 (with an average concentration of 27% in mass) it varies from $390 \text{ W m}^{-2} \text{ K}^{-1}$ to $735 \text{ W m}^{-2} \text{ K}^{-1}$ showing a small difference (which is within the Standard Estimated Error of about $\pm 45 \text{ W m}^{-2} \text{ K}^{-1}$) between the two scenarios. In fact with a compacted bed, the carbon grains have more physical contacts with the wall (estimated to be up to 85% wall surface area) than the gas contact with the wall: the contribution of convective heat transfer to the wall contact heat transfer is not predominant. Therefore the presence of refrigerant or no refrigerant in the packed activated carbon bed has limited effect on the estimated wall contact heat transfer coefficient: this heat transfer with refrigerant is estimated to be about 15% on average (with a maximum value of 30%) better than with no refrigerant.

The heat transfer properties of a packed granular activated carbon bed based on density ρ (kg m^{-3}) and refrigerant average concentration x_a (kg kg^{-1}) is highly useful for modelling and designing with confidence tubular generators for Adsorption Refrigeration and Heat pump applications. By assuming a linear variation of parameters (slope, constant and SEE) of the best fitted line equations (see **Figure 12** and **Figure 13**) with refrigerant concentration at constant packed bed density, both thermal conductivity of the packed bed (λ) and wall contact heat transfer coefficient (h) including the Standard Estimated Error (SEE) are given by expressions summed up in **Table 4**.

Table 4: Heat transfer properties vs. packed bed density and R723 average concentration.

$$(500 \text{ kg m}^{-3} < \rho < 800 \text{ kg m}^{-3} \text{ and } 0 \text{ kg kg}^{-1} \leq x_a < 0.354 \text{ kg kg}^{-1})$$

Properties	Estimated Equations
λ ($\text{W m}^{-1} \text{ K}^{-1}$)	$\lambda = (0.001 + 0.012 x_a) \rho - (0.2679 + 5.73 x_a)$ SEE = $\pm (0.011 + 0.144 x_a)$
h ($\text{W m}^{-2} \text{ K}^{-1}$)	$h = (3.4 - 2.6 x_a) \rho - (1870 - 2033 x_a)$ SEE = ± 17

4. Conclusions and perspectives

The wall contact heat transfer coefficient (h) and packed activated carbon thermal conductivity (λ) have been estimated by using a combined numerical heat conduction method and iterative process based on minimizing the Mean Square Error (MSE) between experimentally measured and model predicted temperatures. The packed granular activated carbon (GAC) also contains R723 refrigerant with a maximum average concentration of 0.27 kg kg^{-1} . For the four test samples with packed bed density ranging from 500 kg m^{-3} to 800 kg m^{-3} , the results show a quasi-linear increase of both thermal conductivity (λ) and wall contact heat transfer coefficient (h) with the packed bed density: the thermal conductivity of packed GAC-R723 refrigerant pair is $0.77 \text{ W m}^{-1} \text{ K}^{-1} < \lambda < 1.36 \text{ W m}^{-1} \text{ K}^{-1}$ (about three times the values without R723 refrigerant) while the wall contact heat transfer coefficient is $390 \text{ W m}^{-2} \text{ K}^{-1} < h < 735 \text{ W m}^{-2} \text{ K}^{-1}$ (up to 30% better than values without R723 refrigerant). This has led to the establishment of a correlation between each heat transfer property (λ or h) and both packed granular activated carbon (GAC) density and maximum average concentration of R723 refrigerant: this is highly useful for future modelling and design of tubular generators for Adsorption Refrigeration and Heat pump applications.

Acknowledgments

The project was supported by EPSRC (Grant EP/J000876/1) and Chemviron Carbons Ltd (Lockett Road, Lancashire WN4 8DE, UK).

References:

- [1]. Argo, W. B., and J. M. Smith, "Heat Transfer in Packed Beds: Prediction of Radial Rate in Gas-Solid Beds," *Chem. Eng. Prog.*, 1953; 49: 443-454.
- [2]. S. Yagi, D. Kunni, Studies on effective thermal conductivities in packed beds, *A.I.Ch.E. Journal*, 1957; 3: 373-381.
- [3]. Calderbank, P. H., and L. A. Pogorski, "Heat Transfer in Packed Beds," *Trans. Inst. Chem. Engrs.*, 1957; 35: 195-202
- [4]. A.V. Luikov, A.G. Shashkov, L.L. Vasiliev, Yu. E. Fraiman, Thermal conductivity of porous systems, *International Journal of Heat and Mass Transfer*, 1968; 11(2): 117–140.
- [5]. G.J. Cheng, A.B. Yu, P. Zulli, Evaluation of elective thermal conductivity from the structure of a packed bed, *Chemical Engineering Science*, 1999; 54(19): 4199–4209.
- [6]. K. Ofuchi, D. Kunii, Heat transfer characteristics of packed beds with stagnant fluids, *International Journal of Heat and Mass Transfer*, 1965; 8(5): 749-757.
- [7]. E. Tsotsas and H. Martin, Thermal conductivity of packed beds: A review, *Chemical Engineering and Processing: Process Intensification*, 1987; 22(1): 19-37.
- [8]. Z. Tamainot-Telto, R.E. Critoph, Adsorption refrigerator using monolithic carbon-ammonia pair, *International Journal of Refrigeration*, 1997; 20(2): 146-155.
- [9]. Z. Tamainot-Telto, Novel explanation of Dubinin-Astakhov theory in sorption reactors design for refrigeration and heat pump application, *International sorption heat pump conference, ISHPC 2014*, March 31 – April 2, 2014, Washington DC-USA; Paper No.84.
- [10]. R. E. Critoph, Adsorption Refrigerators and Heat Pumps, Chapter 10, pp. 303-340, *Carbon Materials for Advanced Technologies*, Ed. Timothy D Burchell, Pub. Pergamon, 1999
- [11]. M. Khaliji Oskouei and Z. Tamainot-Telto, Effect of packing density on thermal properties of granular activated carbon packed bed by using of inverse heat conduction method, *Proc. 10th International Conference on Heat Transfer, Fluid Mechanics and Thermodynamics (HEFAT2014)*, Orlando, Florida, 14 - 16 July, Number 1569892091, pp. 1-5.
- [12]. Oluyemi O. Jegede, R. E. Critoph, Extraction of heat transfer parameters in active carbon–ammonia large temperature jump experiments, *Applied Thermal Engineering*, 2016; 95: 499-505

Appendix-A:

First region or outer boundary node:

The node ($i = 3$) in **Figure A.1** is located on the carbon surface, which is in contact with the steel body of the cylindrical holder from the inside. Therefore, heat transfer from the steel wall to that node is a combination of conduction through the steel wall and conduction through the voids between the steel wall and the first layer of packed carbon, which is called contact resistance. **Equations A.1** and **A.2** are the overall heat transfer coefficient which the heat flow faces while travelling through the energy balance lines to the cell boundaries in **Figure A.1**.

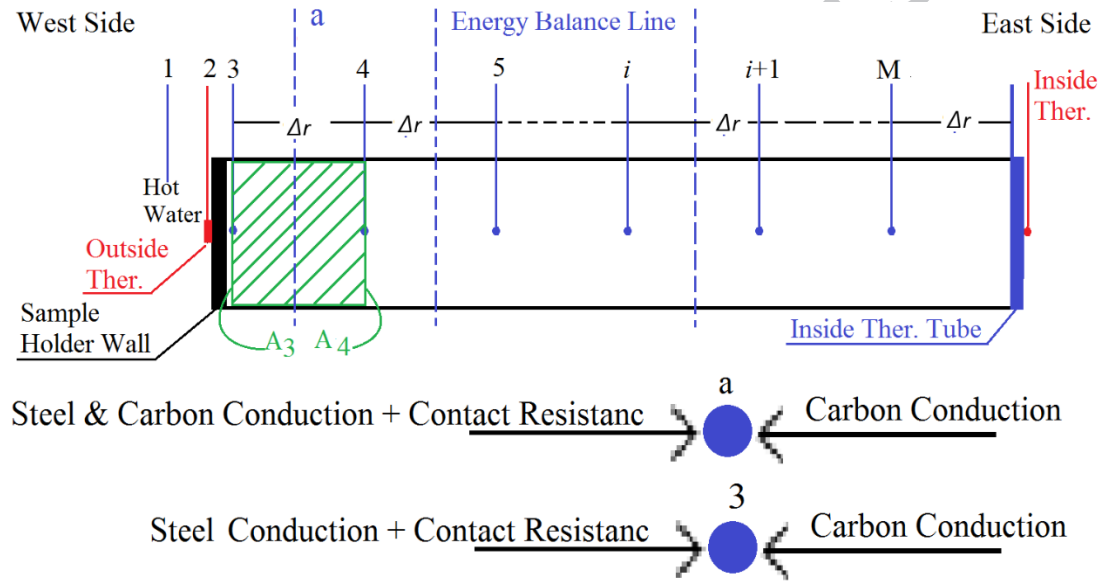


Figure A.1. Domain discretization for energy balance at the carbon packed outer boundary. Heat transfer mechanism into the boundary node and energy balance line with delimiting of the control volume (A_3 , A_2); Δr is a radial increment.

$$\begin{array}{l} \text{Steel Conduction} \\ \text{Convection} \\ \text{Carbon Conduction} \end{array} \rightarrow UA_{west} = \frac{A_3}{\frac{t_w}{2} + \frac{\Delta r/2}{\lambda_{Steel}} + \frac{\Delta r/2}{\lambda_{Carbon}}} \quad (\text{A.1})$$

$$\text{Carbon Conduction} \rightarrow UA_{east} = \frac{A_4}{\Delta r / \lambda_{Carbon}} \quad (\text{A.2})$$

$$A_3 = 2\pi r_3 L_C \quad r_3 = \frac{ID}{2} \quad (\text{A.3})$$

$$A_4 = 2\pi r_4 L_C \quad r_4 = \frac{ID}{2} - \Delta r \quad (\text{A.4})$$

Mass of carbon for repressing cell is:

$$M_{3-carbon} = \pi(r_3^2 - r_4^2) \times \rho_{Carbon} \times L_C \quad (A.5)$$

Second regions or internal nodes:

Equations A.6 and **A.7** show that the only resistance which the heat flow is confronted with while travelling towards the energy base lines over the specific control volume is the carbon packed conduction resistance (**Figure A.2**). Therefore, the overall heat transfer from the west and east boundaries for the internal nodes is just heat conduction through the carbon packed bed.

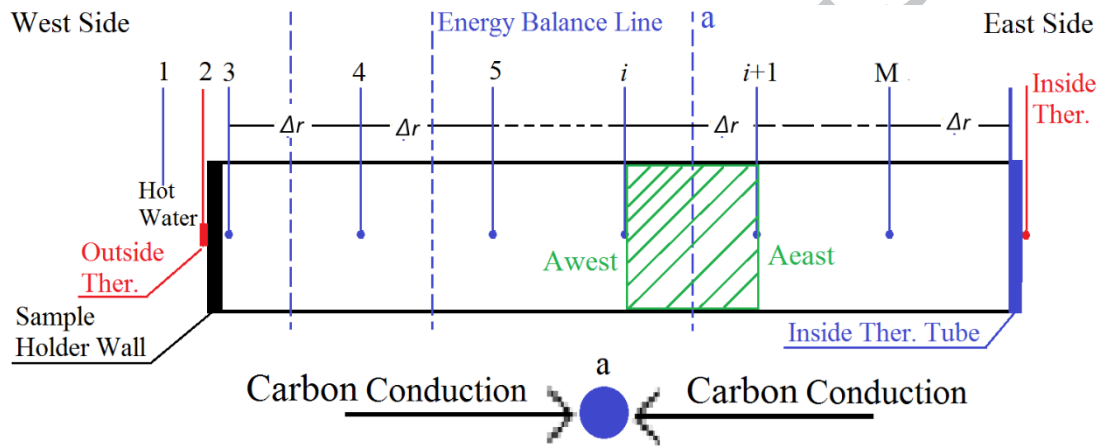


Figure A.2. Domain discretization for energy balance at the carbon packed bed for the inner nodes. Heat transfer mechanism to the boundary node and energy balance line with delimiting of the control volume (A_i); Δr is a radial increment.

$$\text{Carbon Conduction} \rightarrow UA_{west} = \frac{A_i}{\Delta r / \lambda_{Carbon}} \quad (A.6)$$

$$\text{Carbon Conduction} \rightarrow UA_{east} = \frac{A_{i-1}}{\Delta r / \lambda_{Carbon}} \quad (A.7)$$

$$A_i = 2\pi r_i L_C \quad r_i = \frac{ID}{2} - (i - 3)\Delta r \quad (A.8)$$

The mass of the carbon for the representing cells is:

$$M_{i-carbon} = \pi(r_i^2 - r_{i+1}^2) \times \rho_{Carbon} \times L_C \quad (A.9)$$

Third region or centre node:

The centre node is allocated in the middle of the sample reactor, where the internal thermocouple was located (**Figure A.3**). Because of the symmetry condition in the sample cylinder, **Equation A.10** shows that the heat flow through the centre cell is from the west boundary, and that it is purely heat conduction through the carbon packed bed. **Equation A.11** shows no heat transfer from the east boundary because of the assumption of an adiabatic condition.

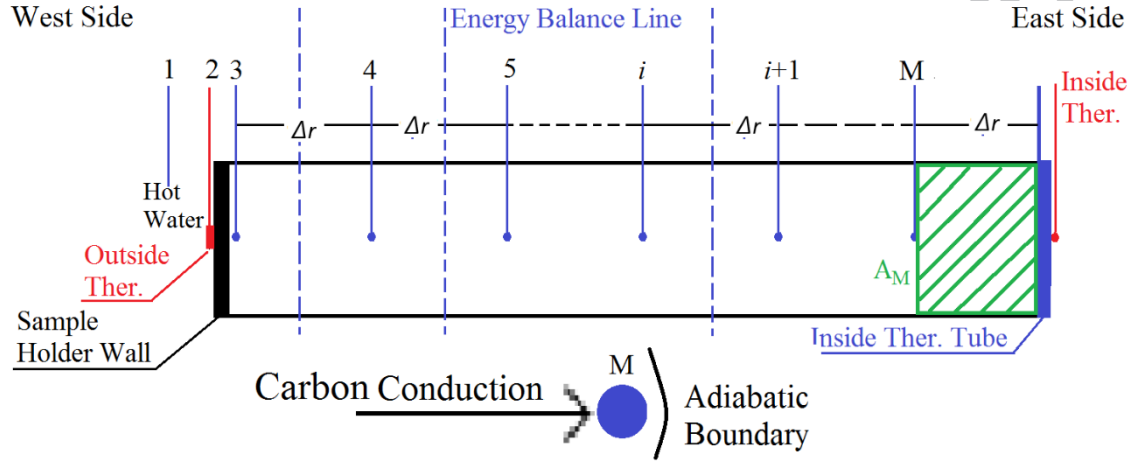


Figure A.3. Domain discretization for energy balance at the carbon packed bed for the centre node. Heat transfer mechanism to the centre node and energy balance line with delimiting of the control volume (A_M); Δr is radial increment.

$$\text{Carbon Conduction} \rightarrow UA_{west} = \frac{A_M}{\Delta r / \lambda_{carbon}} \quad (\text{A.10})$$

$$\text{Adiabatic Boundary} \rightarrow UA_{east} = 0 \quad (\text{A.11})$$

$$A_M = 2\pi r_M L_C \quad r_M = \Delta r \quad (\text{A.12})$$

Mass of carbon for representing cell is:

$$M_{M-carbon} = \pi \left(r_M^2 - \frac{D_o^2}{4} \right) \times \rho_{carbon} \times L_C \quad (\text{A.13})$$

Appendix-B:

In **Equations 2** and **11**, $\Delta T/\Delta t$ and $\Delta T_{sat}/\Delta t$ change with temperature and saturation temperature (or pressure) for the represented cells over the time. Therefore, the discretized models are:

$$\frac{\Delta T}{\Delta t} = \frac{T_i^{t+1} - T_i^t}{\Delta t} \quad \text{and} \quad \frac{\Delta T_{sat}}{\Delta t} = \frac{T_{sat}^{t+1} - T_{sat}^t}{\Delta t} \quad (\text{B.1})$$

$$UA\Delta T =$$

$$M_{Carbon}(CP) \frac{\Delta T}{\Delta t} - M_{Carbon} \left(RA \frac{T}{T_{sat}} \right) \left[-\frac{Kn\alpha}{T_{sat}} \left(\frac{T}{T_{sat}} - 1 \right)^{n-1} \right] \frac{\Delta T}{\Delta t} -$$

$$M_{Carbon} \left(RA \frac{T}{T_{sat}} \right) \left[Kn\alpha \frac{T}{T_{sat}^2} \left(\frac{T}{T_{sat}} - 1 \right)^{n-1} \right] \frac{\Delta T_{sat}}{\Delta t} \quad (\text{B.2})$$

$$\rightarrow \frac{UA\Delta T}{M_{Carbon}} + \left(RA \frac{T}{T_{sat}} \right) \left[Kn\alpha \frac{T}{T_{sat}^2} \left(\frac{T}{T_{sat}} - 1 \right)^{n-1} \right] \left(\frac{T_i^{t+1} - T_i^t}{\Delta t} \right) =$$

$$\left[(CP) - \left(RA \frac{T}{T_{sat}} \right) \left[-\frac{Kn\alpha}{T_{sat}} \left(\frac{T}{T_{sat}} - 1 \right)^{n-1} \right] \right] \left(\frac{T_{sat}^{t+1} - T_{sat}^t}{\Delta t} \right)$$

(B.3)

$$\rightarrow \frac{\frac{UA\Delta T}{M_{Carbon}} \Delta t + \left(RA \frac{T}{T_{sat}} \right) \left[Kn\alpha \frac{T}{T_{sat}^2} \left(\frac{T}{T_{sat}} - 1 \right)^{n-1} \right] (T_{sat}^{t+1} - T_{sat}^t)}{(CP) - \left(RA \frac{T}{T_{sat}} \right) \left[-\frac{Kn\alpha}{T_{sat}} \left(\frac{T}{T_{sat}} - 1 \right)^{n-1} \right]} = T_i^{t+1} - T_i^t \quad (\text{B.4})$$

$$\rightarrow \frac{\frac{UA\Delta T}{M_{Carbon}} \Delta t + \left(RA \frac{T_i^t}{T_{sat}^t} \right) \left[Kn\alpha \frac{T_i^t}{T_{sat}^t} \frac{T_i^t}{T_{sat}^t} \left(\frac{T_i^t}{T_{sat}^t} - 1 \right)^{n-1} \right] (T_{sat}^{t+1} - T_{sat}^t)}{(CP) - \left(RA \frac{T_i^t}{T_{sat}^t} \right) \left[-\frac{Kn\alpha}{T_{sat}^t} \left(\frac{T_i^t}{T_{sat}^t} - 1 \right)^{n-1} \right]} + T_i^t = T_i^{t+1} \quad (\text{B.5 or 13})$$

Highlights:

- The thermal properties of packed granular activated carbon (GAC) and Ammonia Blend refrigerant (R723) are evaluated.
- A numerical method combined with experimental data was used.
- The thermal conductivity varies from 0.77 and 1.36 $W m^{-1} K^{-1}$.
- The thermal conductivity is about three times the values without R723 refrigerant.
- The wall contact heat transfer coefficient varies between 390 and 735 $W m^{-2} K^{-1}$ and is up to 30% better than values without R723 refrigerant.